Detailed catalyst layer structure of Proton Exchange Membrane Fuel Cell from contrast variation small-angle neutron scattering

Florian Chabot, Jongmin Lee, Florent Vandenberghe, Laure Guetaz, Gérard Gebel, Sandrine Lyonnard, Lionel Porcar, Sébastien Rosini, Arnaud Morin

Detailed catalyst layer structure of Proton Exchange Membrane Fuel Cell from contrast variation small-angle neutron scattering

Florian Chabot[a], Jongmin Lee[a], Florent Vandenberghe[a], Laure Guétaz[a], Gérard Gebel[a], Sandrine Lyonnard[c], Lionel Porcar[b], Sebastien Rosini[a], Arnaud Morin[a]*

[a]Univ. Grenoble Alpes, CEA, Liten, DEHT, 38000 Grenoble, France

[b]Institut Max Von Laue-Paul Langevin (ILL), 71 Avenue des Martyrs, 38042 Grenoble, France

[c]Univ. Grenoble Alpes, CEA, CNRS, IRIG, SyMMES, 38000 Grenoble, France

*Email: arnaud.morin@cea.fr

Keywords: PEMFC, protonic conductor, ionomer, SANS, catalyst, electrode, water

Abstract :

Despite significant decrease in past decades, the cost of Proton Exchange Membrane Fuel Cell (PEMFC), largely due to the rare and expensive electro-catalyst made of platinum, restrains its massive deployment. Therefore, reducing the platinum content in the electrode is the keystone of intense research efforts to increase catalyst activity or utilisation. Catalyst layer structure, and especially the water and ionomer distributions, rule the active sites availability for electrochemical reactions, and thus catalyst utilisation, because of their influence on the transport of protons and oxygen. However, the rational design of more efficient electrodes faces the lack of accurate knowledge of its complex nanoporous structure. Specifically, ionomer and water distribution are very difficult to probe with conventional electron microscopy or X-Ray techniques. This work provides quantitative information on electrode structure, regarding ionomer and water distributions thanks to an extensive analysis of Small Angle Neutron Scattering (SANS) profiles at different relative humidity (RH) and contrast. A 2 to 3 nm thin ionomer film spreads around the Pt/C catalyst particles while a condensed water layer appears at the catalyst/ionomer interface depending on the type of carbon support.

1. Introduction

Catalyst layers host electrochemical reactions and drive the overall conversion efficiency of Proton Exchange Membrane Fuel Cell (PEMFC). The best state-of-the-art catalyst layer is a complex porous nanostructured material (often referred to as electrode) allowing the transport of gaseous reactants, protons and electrons, as well as heat and water generated during the electrochemical reactions. It is made of platinum (Pt) nanoparticles (2-5 nm), bearing the electro catalytic sites supported on carbon particles, of approximate size around 10 to 40 nm, ensuring the electronic conductivity. These Pt/Carbon catalyst particles agglomerate to create a porous network, covered by a proton conducting polymer[1] which forms either thin film coating, typically from 5 to 20 nm[2], either agglomerates larger than 150 nm. The latter partially fills the pores[3].

This proton conducting polymer is also called "ionomer". Along with water, it plays a crucial role in the catalyst layer operation by transporting protons between the membrane and the active sites, a process that directly depends on hydration[4]. However, by filling the pores, the ionomer decreases reactive gases diffusivity inside the catalyst layer.[5,6] Moreover, by coating the catalyst, it may act as a barrier for reactants to reach active sites[7–9] and, additionally, it can specifically adsorb on the active sites, therefore blocking the electrochemical reaction[8]. All these phenomena can dramatically impact fuel cell operation, especially at the cathode side where slow Oxygen Reduction Reaction (ORR) kinetics and low oxygen diffusion coefficient are the two major causes of performance losses[9–11]. Because transport and reaction kinetic limiting phenomena are coupled, the operation in the catalyst layer is heterogeneous, and the current is mostly produced by only a small fraction of the catalyst layer volume[12,13]. To summarize, increasing ionomer content enhances protonic conductivity while decreasing oxygen diffusivity, thus optimizing its incorporation is critical to improve fuel cell performances.

The state-of-the-art proton conductor used in PEMFC catalyst layers is a perfluorinated sulfonic acid (PFSA) ionomer. PFSA membranes have been extensively studied in past decades[4,14–17]. The general chemical structure of PFSA is presented in **Figure S1** in the Supporting Information. The ionomer is composed of two parts: the perfluorinated hydrophobic polymer backbone and the pendent side-chains ending with hydrophilic sulfonic acid groups (SO_3^-). As illustrated in **Figure 1-a**, the combined presence of both highly hydrophobic and hydrophilic groups leads to nano phase separation between the polymer and the aqueous phase in which proton transport occurs[18]. The aggregation of polymer backbones induces flat lamella-like

structures with an average thickness estimated around 2.7 nm[15] for Nafion® membrane. These lamellae are roughly stacked together in parallel within certain local ordering to form randomly oriented bundles of hundred of nanometers. It is well known that water uptake, proton conductivity and oxygen permeability of the ionomer are closely related to its chemical structure[19]. Specifically, the different PFSA structures are defined through their Equivalent Weight (EW) as summarized by Kusoglu *et* Weber[18].

The behavior and properties of bulk ionomer membranes are well known whereas the role and state of ionomer inside catalyst layers have been under-evaluated until recently. It has been demonstrated that ionomer thin films (<50 nm) do not exhibit the same properties as bulk material[19]. Indeed, the ionomer thin film conductivity and dioxygen permeability are lower than for membrane[9,19–22] due to the ionomer structural reorganization occurring in the vicinity of the substrate material described by Woo *et al.*[23], depends on the substrate material[24]. Even though *ex-situ* characterizations on model flat substrates bring valuable information on the structure and properties of ionomer thin films, they are most probably not representative to the actual state in a catalyst layer. Indeed, there are too few *in situ* structural studies on the ionomer to have a clear understanding of its structure and properties inside the catalyst layer, especially upon hydration. Thereby, additional *in-situ* characterization are essential to link the ionomer structure to fuel cell performance. In this objective, several authors have developed techniques to characterize the ionomer distribution inside catalyst layers by transmission electron microscopy (TEM) tomography[1] or atomic force microscopy (AFM)[3]. Another valuable technique used in the past years to study catalyst layer structure is small angle scattering (SAS). Myers *et al.*[25] used small angle X-Ray scattering (SAXS) to study the platinum nanoparticles sizes distribution, taking advantage of the strong interactions between X-rays and heavy elements. However, it is difficult to extract the ionomer structure from 1D SAXS profiles because the ionomer contribution to the scattering intensity is very low as compared to platinum signal. In contrast to X-Rays, neutrons are sensitive to nuclei and the scattering contribution from platinum is negligible in comparison to carbon and ionomer contributions. Hence, Small Angle Neutron Scattering (SANS) appears as the best technique to study the ionomer structure inside catalyst layers. Koizumi *et al.*[26] performed ex-situ characterizations of electrodes by SANS. More recently, Lee *et al.*[27] used SANS to relate fuel cell operation with the ionomer hydration in a real operating electrode. In addition, Harada and co-workers used contrast variation to study ionomer adsorption at the catalyst surface within inks[28,29] and electrodes[30]. However, despite these studies, there is still no

straightforward method to unravel the water dependent catalyst layer structure from 1D SANS profiles due to complex multiscale heterogeneous structures.

In this work, we propose 1D SANS profiles analysis highlighting structural information on catalyst layer, and specifically on the distribution of the ionomer and water, as a function of relative humidity and using contrast variation. The method was applied to study the influence of the electrode manufacturing process and the type of carbon support, e.g. Vulcan or High Specific Area (HSA), on the ionomer structure and water distribution on two electrodes made from Nafion® (1000 EW) and 50% weight Platinum over Carbon catalyst (Pt/C). The *ex-situ* method is applicable to a wide range of catalyst layer composition and provides invaluable insights into nanoscale electrode structure-to-device operation relationship in PEMFC.

2. Experimental

2.1. Samples specifications

Three types of electrodes were manufactured in order to study the influence of the dispersion process and the type of carbon support on the structure of the catalyst layer, and more specifically, the ionomer dispersion, structure and swelling behavior. Electrodes did not operate, thus they should be either cathode or anode.

ND- Vulcan (ND for Non Dispersed): the ink was prepared using 50% weight platinum supported on Vulcan carbon (TEC10V50E from Tanaka) with Nafion® D2020 (EW = 1000 $g.mol_{SO3-}^{-1}$) dispersion provided by Dupont DeNemours. The ink dry content was 17% weight. Water is added first on the catalyst powder, then the ionomer dispersion and finally pure ethanol. Ionomer dispersion solvent is a water/2-propanol mixture (20/75%). The ink was then left twenty-four hours under magnetic stirring. Then, it was deposited onto a PTFE substrate using bar coating. Finally, Membrane Electrode Assembly (MEA) was obtained by hot pressing electrode on N115 membrane at 160°C and 2 MPa for 10 minutes.

D- Vulcan (D for Dispersed): the ink was prepared with TEC10V50E and Nafion D2020. In order to improve the ionomer dispersion compared to the previous ink (ND- Vulcan), the catalyst was first dispersed into a mixture of Diacetone Alcohol (DAA) and ultrapure water. Then, the Nafion dispersion was added. The catalyst ink was mixed before and after ionomer addition with a planetary mixer (Kurabo). Next, the ink was stirred with milling balls onto a roller mixer for 24 hours, before being sprayed onto a PTFE sheet. The ink dry matter content was 2% weight.

D- HSA - supplied: MEA was manufactured and provided by Toyota Motor Europe (TME) in the frame of the European project Further-FC[31]. The ink was prepared from Nafion D2020 and TEC10E50E catalyst from Tanaka, which is a catalyst with 50% weight platinum supported on High Specific Area (HSA) carbon. Catalyst powder was dispersed into ultrapure water and then mixed with a planetary mixer. Next, the ink was mixed again after adding Nafion and DAA. The dry matter content was 10% weight. The catalyst layer was prepared by bar coating a PTFE substrate and then transferred by hot pressing on a NC700 membrane from Dupont DeNemours. **Table S1** gives more details on samples composition and manufacturing. Schemes on **Figure 1-b** represents main samples features. Two main characteristics differentiate the electrodes: first, the improved dispersion process used for "Dispersed (D)" catalyst inks, represented by the red arrow, and second, the type of carbon support that is represented by a smooth sphere for Vulcan and by a spherical particle with a rough surface for the HSA nanoporous particles. In the following, those schemes will be used in figures as a guide to distinguish electrodes called ND- Vulcan (Non-dispersed), D- Vulcan (Dispersed) and D- HSA (Dispersed). Thus, in the following, on the one hand, comparison of D- Vulcan and ND- Vulcan electrodes exhibits structural evolutions induced by the manufacturing process, while, on the other hand, D- Vulcan and D- HSA electrodes comparison shows the carbon support key role for the electrode structure.

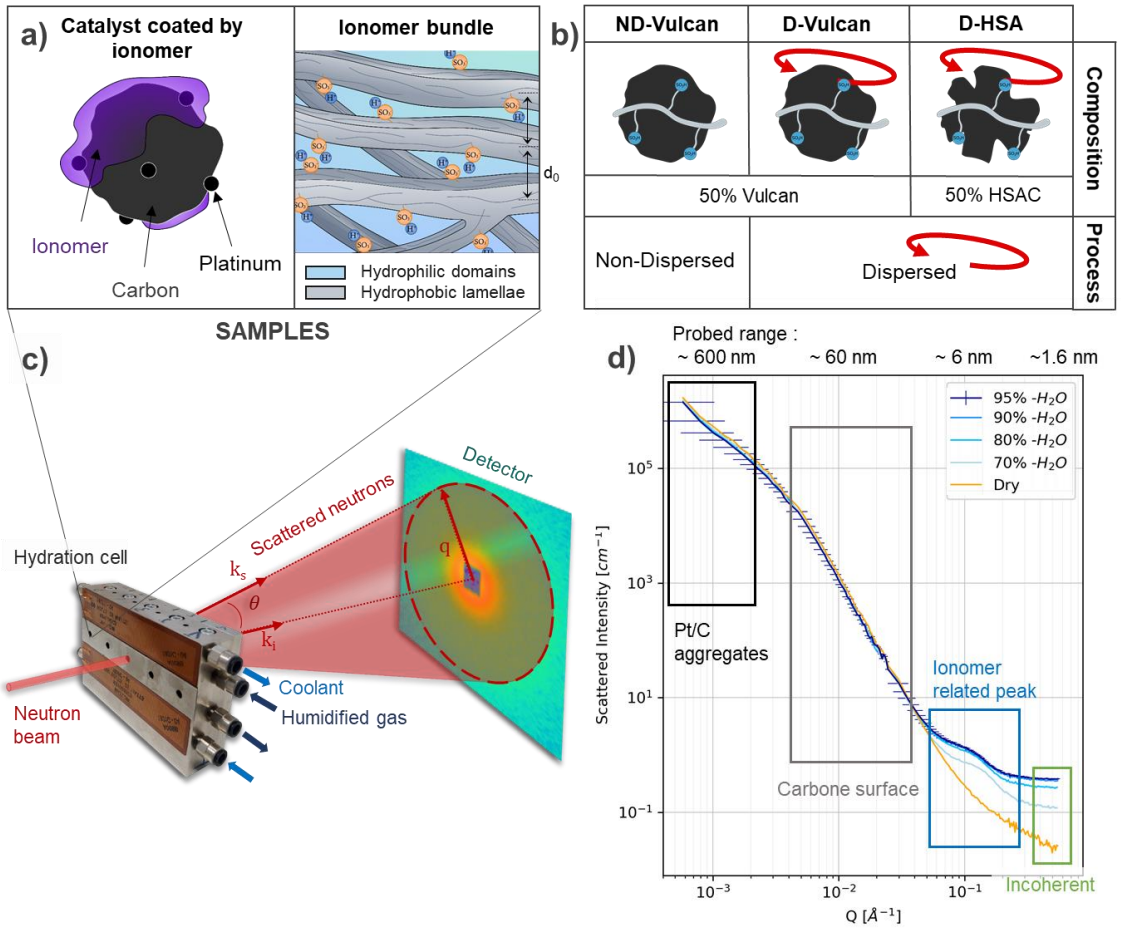

Figure 1. a) Schematic representation of structures probed with SANS; electrode building block made from Pt/Carbon aggregates covered with thin ionomer films; Ionomer bundles present in bulk membrane or in the large aggregates (~150 nm) with nano phase separation between hydrophobic and hydrophilic domains. b) Main characteristics of the three electrodes studied with their associated schemes representing the type of carbon support, the ionomer and the use of improved dispersion process (red arrow). c) Illustration of the experimental set-up for in-situ acquisition of 1D SANS profiles of catalyst layers and membranes. $\overrightarrow{k_i}$ being the neutrons incident wave vector, $\overrightarrow{k_s}$ the scattered neutrons wave vector and $\vec{q}$ the scattering vector. d) 1D SANS profiles of ND- Vulcan electrode for several relative humidity and characteristic sizes of probed structures. Measurements errors on intensity and angles (Q) are represented only on the first SANS profile.

2.2. SANS Technique

Small angle neutron scattering (SANS) probes structures with characteristic sizes from the nanometer to the micron. Collimated neutrons beam scatters at specific angles values after interacting with a sample. Scattered neutrons intensity is proportional to the volume fraction of

particles within the sample and to the contrast factor between the particle and the surrounding medium, squared. Contrast factor is the difference between two materials in Scattering Length Density (SLD), which is an intrinsic property. In the present case, the SLD of the flowing gas was controlled by the level of deuteration present in the water solvent controlling the gas humidity. As presented in **Figure 1-c**, a flat 2D detector collects scattered neutrons intensities at a defined distance from the sample. Then, for isotropic materials, azimuthal scattered intensities averaging leads to 1D SANS profile. It is a plot of the average scattered intensity as a function of the modulus of the scattering vector q (in $Å^{-1}$) related to the scattering angle θ and λ the incident neutrons wavelength in Å through Equation 1.

$$q = \frac{4\pi . \sin(\theta/2)}{\lambda} \quad (1)$$

Figure 1- d presents typical 1D SANS profiles from ND- Vulcan electrode for different relative humidity conditions. In our experimental configuration, 1D SANS profiles probe structures ranging from almost 1 nm to roughly 500 nm and exhibit four significantly distinct regions that give different structural information as presented by the **Table 1**. As shown by the calculated probed range on the top y-axis of the plot, large structures scatter at low q values whereas small ones scatter at high q values. In our samples, the platinum volume fraction is estimated to be around 4% and its scattering length density ($\rho = 6.3.10^{-6}$ $Å^{-2}$) is close to the SLD of carbon ($\rho = 6.7.10^{-6}$ $Å^{-2}$). Thus, we consider the platinum contribution to the SANS profile cannot be distinguished from that of carbon, and is even negligible. For SANS experiments on powder (as the catalyst layer), the solvent is the air hydrated either with H_2O or D_2O.

Table 1. Description of information obtained from a SANS profile of catalyst layer at different q ranges.

q range *[$Å^{-1}$]*	Materials and structures probed
$q < 5.10^{-3}$	Profiles give information on the large Pt/Carbon catalyst aggregates structure.
$5.10^{-3} < q < 5.10^{-2}$	The intensity decreases as a q^{-n} function, with n a value around 4 related to the carbon surface and its roughness.
$1.10^{-1} < q < 2.10^{-1}$	Profiles of hydrated catalyst layers exhibit a peak of a well-defined structure of few nanometers, which is related to ionomer.
$q > 3.5.\ 10^{-1}$	Scattered intensity mainly comes from the incoherent scattering that depends on the sample composition. Due to high incoherent scattering of hydrogen atoms, intensity gives information on the total hydration level of the sample.

In the following, SANS profiles are corrected from the incoherent scattering. Incoherent scattering intensity is measured at 0,4 A^{-1} and subtracted to the scattering intensity on the whole Q range. Hence, SANS profiles evolution with relative humidity or contrast variation would be related to sample structure.

2.3. SANS Setup

SANS experiments[32,33] were performed at the beamline D22[34] of the Institut Laue-Langevin (ILL). The catalyst layer was recovered by gently scratching catalyst layer deposit with a surgical blade. We checked by electronic microscopy that the surface of the membrane was not scratched and that only catalyst layer was collected. However, it is difficult to recover the whole catalyst layer thickness, a thin layer remains on the membrane surface. The recovered powder was then loaded in a titanium cell without any additional treatment to avoid any modification of the nanostructured catalyst layer. The cell, presented in **Figure 1-c**, was designed specifically for SANS measurements. It allows to control the temperature and relative humidity for five samples in parallel by N_2 flushing with dew point monitored and controlled by a homemade bench. Cell compartments diameter and depth are respectively 3 mm and 200µm. **Table 2** presents the several SANS configurations used in order to record profiles with good resolution when needed and good statistic in a broad q range from 5.10^{-1} to 5.10^{-4} A^{-1} characterizing structures ranging from 1 nm to 1 µm. The beam diameter is 3 mm.

Table 2. Experimental configurations used for 1D SANS profiles acquisition of the three electrodes studied.

	ND- Vulcan electrode		**D- Vulcan & ND- HSA electrodes**		
Configuration	1^{st}	2^{nd}	1^{st}	2^{nd}	3^{rd}
Wavelength [Å]	5	5	6	6	11
Sample to Collimator Distance [m]	2	17.6	2.8	17.6	17.6
Sample to Detector Distance [m]	2.8	17.6	3.1	17.6	17.6
Counting Time [min]	2	5	5	5	5

2.4. SANS correction and reduction

Grasp Software[35] developed by the ILL was used for data correction and reduction as presented by Hammouda[36]. Data with were merged between configuration and analyzed. As the sample is a powder, the quantity of material inside the 6 mm x 200 µm cavity cannot be

determined with accuracy, such that average sample thickness is not really known. As a result, profiles cannot be normalized by the material thickness value, which is set to 200 µm corresponding to the depth of the cavity in which the sample is loaded. Since the total quantity of material is not controlled in each cell, the overall scattered intensity differs from one sample to another. In order to get rid of the difference in material amount between samples, the invariant Q_v in $Å^{-4}$ for each dry sample was computed following Equation 2. Its value is directly proportional to components volume fractions[36].

$$Q_v = \frac{1}{2\pi^2}\int_{-\infty}^{+\infty} I(q)q^2.dq \quad (2)$$

Experimentally, the invariant is computed over the q range of the profiles, so at least on three orders of magnitude. Hence, it is assumed that it gives a good approximation of the theoretical invariant. Finally, each 1D SANS profile intensities were multiplied by the ratio of their dry invariant over one dry sample chosen arbitrary as a reference.

2.5. SANS profiles simulation

In the following, ideal core shell sphere models are used to simulate SANS profiles from the catalyst layer primary particles. Authors have already used those models to study the catalyst/ionomer interaction in catalysts inks[37,38]. Simulation and fitting of experimental data were realized with SASView Software[39]. Equation 3 presents the form factor $P(q)$ in cm^{-1} for a simple core shell model[40] that could be extended to several shells.

$$P(q) = \frac{\varphi}{V}.F^2(q) + background \quad (3)$$

Where,

$$F(q) = \frac{3}{V_{s1}}.[\,3V_c(\rho_c - \rho_1)\frac{\sin(q.r_c) - \mathrm{q}.r_c\cos(q.r_c)}{(q.r_c)^3} + \sum_1^s 3V_s(\rho_\mathrm{s} - \rho_{\mathrm{s}+1})\frac{\sin(q.r_\mathrm{s}) - q.r_s\cos(q.r_s)}{(q.r_s)^3}\,] \quad (4)$$

With c standing for the core (carbon particle) and s for the number of shells. Thus, r_s is the sum of the core radius, r_c, and the shell thickness. φ being the scale factor, V the volume ($Å^3$), ρ the scattering length density ($Å^{-2}$) and r the radius (Å).

2.6. Trasnmission electronic microscopy

In order to image the ionomer distribution within the two CLs, the MEA cross-section were analyzed by transmission electron microscopy (TEM). For these analyses, the MEA samples

were embedded in epoxy resin and thin slices of around 100 nm thick were cut by ultramicrotomy and deposited on a copper TEM grid. Observations were performed on a FEI-Themis microscope operated at 200 kV and equipped with probe corrector and X-EDS spectrometer composed of 4 SiliconDrift Detectors. The fluorine EDS elemental map were recorded on the two samples using the same experimental conditions (beam intensity, pixel size, acquisition time) in order to expose the sample to the same electron dose[41].

3. Results and discussion

3.1. Impact of manufacturing process on ionomer structure in catalyst layer

Electrodes profiles presented in **Figure 1-d** show a characteristic peak around 0.17 $Å^{-1}$ once the catalyst layer is hydrated. This location corresponds to a characteristic size of the structure probed that is around 4 nanometers. However, even if it roughly corresponds to the diameter of the Pt nanoparticles, this peak could not result from the platinum particles because of their negligible contribution to the total scattered intensity. Moreover, the observed peak appears only upon hydration, increase in intensity and shift to lower q values when increasing the relative humidity. This trend is characteristics of swelling structures. Now, as discussed in the introduction, ionomer phase separation appears as its water content increases with relative humidity, which leads to the so called ionomer peak[4,14,15,42] for the bulk material in the exact same q range. Therefore, one can confidently assume that this peak results from the ionomer inside the catalyst layer, which forms either aggregates (~150 nm) or thin films (5- 15 nm).

Figure 2-a presents recorded 1D SANS profiles of a Nafion membrane N117 (1100 EW) from a previous paper[43] and shows the bulk ionomer behaviour upon hydration. When increasing the relative humidity from 80% to 95% the ionomer peak shifts to lower q and its intensity increases. This is a footprint of ionomer swelling, where the average characteristic size of hydrophilic domains increases with the relative humidity. Indeed, the ionomer peak comes from Bragg diffraction of the periodical organization between hydrophilic and hydrophobic domains. This nanophase separation structure is represented in **Figure 1-a**. Peak position (Q_0) is directly related to the average lamellae inter distance (d_0) through the Bragg Equation, $d_0 = 2\pi/Q_0$[36]. Through SAXS study on membrane ionomer, Kreuer *et al.*[14] showed that ionomer peaks positions from membrane shift to higher q values when decreasing the equivalent weight. They showed also that polymer lamellae average thickness decreases with ionomer equivalent weight from 27 Å for a 1100 EW membrane to 24 Å for a Dow 858 EW membrane. Thus, short side

chains ionomers have larger hydrophilic domains and exhibit higher water uptake than 1000 and 1100 EW ionomers.

Looking at **Figure 2-a**, it is interesting to notice that peaks from membrane N117 and ND- Vulcan electrode are close in shape and in position. Thus, the ionomer in bulk membrane and in the catalyst layer have certainly very similar structure. According to several works[9,19,20,24], thin film structure (<50 nm) differs from bulk material and depends on the substrate material on which ionomer is coated. Therefore, it seems that the ionomer peak from ND- Vulcan electrode results rather from aggregates with a characteristic size larger than 50 nanometers having the same structure and behavior as the bulk membrane ionomer. Profiles on **Figure 2-a** are corrected from the incoherent scattering as discussed in section 2.2.

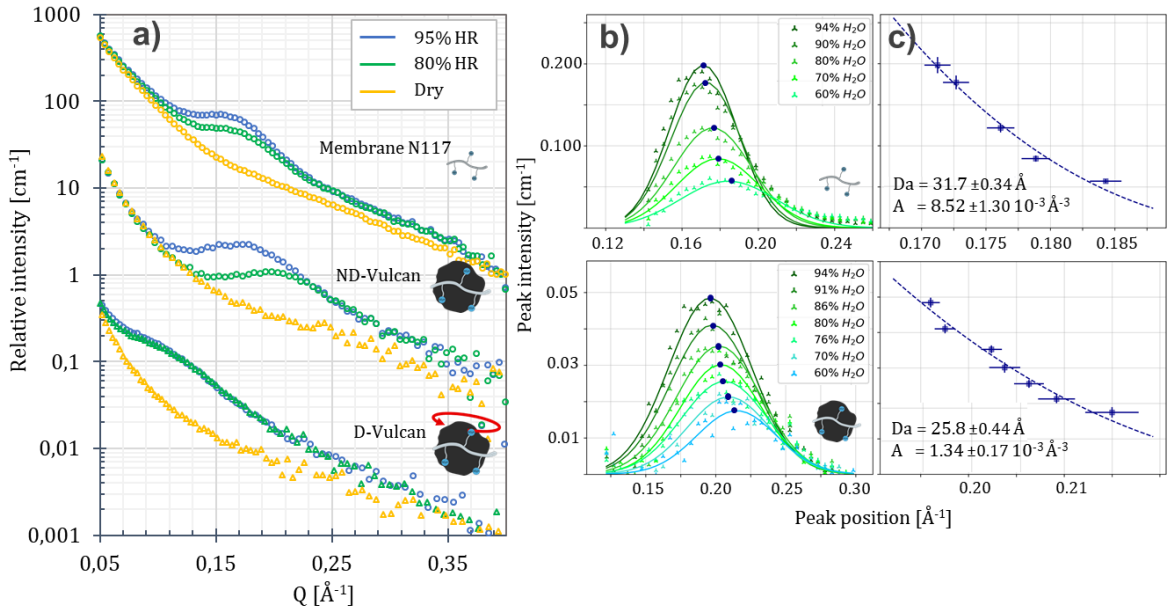

Figure 2. a) Effect of manufacturing process on the ionomer nanostructure contained in catalyst layers. 1D SANS profiles from Nafion N117 membrane is adapted with permission[43]. Copyright 2022, IOP Publishing. ND- Vulcan and D- Vulcan electrodes profiles obtained under dry conditions, 80% and 95% relative humidity. Profiles intensity were multiplied by a factor 10^2 or 10^4 to visually compare profiles from different samples, y-axis is then in relative intensity. Profiles intensity are corrected from incoherent scattering. b) Evolution of the ionomer peak with relative humidity for the N117 membrane and the ND- Vulcan electrode and their fitted Gaussian curves. c) Fit of peaks intensities and positions at several relative humidity with the ideal lamella law model gives the swelling law parameter of the ionomer. D_a is the average thickness of hydrophobic lamella and A is a scale factor.

In order to obtain the ionomer swelling law, several authors[4,15] used Small Angle Scattering (SAS) and isotherm sorption curves to relate lamellae inter-spacing distances and water volume fraction or average number of water molecules per sulfonic group (λ). Hence, Gebel[4] showed that ionomer hydration follows an ideal lamella structure swelling behavior in the range of water content that corresponds to our study. Ideal lamellae are infinitely long structures in comparison to their thickness. Here, the ionomer sorption curve inside the catalyst layer cannot be measured *in-situ.* Indeed, because of the interaction between ionomer and catalyst[44], the water uptake of the catalyst layer for a given relative humidity condition is not the simple sum of the water uptake of the catalyst and of the ionomer.

Based on SAS studies of membranes, the ideal lamella structure behavior of the ionomer will be used in order to obtain swelling laws from the extracted peaks positions and intensities at several relative humidity. This was done with the ND- Vulcan electrode as peaks seem close in shape and in position to the membrane ionomer peaks. Diffraction pattern from an ideal lamella structure follow Equation 5, as presented by Ryiong-Joon Roe[45].

$$I(q) \propto |F(q)|^2 . z\left(\frac{dq}{2\pi}\right) \quad with \quad |F(q)|^2 = (\Delta\rho)^2 . \frac{4}{q^2} sin^2\left(\frac{D_a q}{2}\right) \tag{5}$$

With z equals 1 when the Bragg condition is fulfilled, which corresponds to the maximum peak intensity position. Hence, at the peak maximum position (Q_0), Equation 6 defines the relationship between intensity (I) and position, D_a being the average thickness of the hydrophobic lamellae of polymer in the ionomer. Fitting experimental data with Equation 6 would give the ionomer swelling law that is unique for each ionomer structure.

$$I(Q_0) = \frac{A}{Q_0^2} \, sin^2\left(\frac{D_a Q_0}{2}\right) \tag{6}$$

A term gathers contrast factor and scale unit. Subtraction of the incoherent scattering and the carbon surface slope to the 1D SANS profile allows extracting the ionomer peaks from SANS profiles (see the Supporting Information subsection 2.1 for details). **Figure 2-b** presents the extracted peaks fitted with Gaussians functions for several relative humidity conditions, from 60% to 94% relative humidity for the ND- Vulcan electrode and the Nafion N117 Membrane. Evolutions of peaks intensity and position with hydration are fitted with the ideal lamella structure model defined in Equation 6 and are presented in **Figure 2-c**. Then, polymer lamella average size (D_a) are extracted from fitted curves while their average inter distances are directly related to peaks position through the Bragg law ($d_0 = 2\pi/Q_0$). The hydrophilic domains characteristic sizes (th_{water}) is the difference between d_0 and D_a ($th_{ionomer}$). Ionomer water

uptake strongly depends on the ionomer equivalent weight. In order to compare results obtained with the Nafion 1000 EW to a short side chain ionomer, we performed the same analysis on an electrode made with the same process and composition as ND- Vulcan electrode, but with Aquivion^{TM} (835 EW) instead of Nafion. Details on lamella swelling law are given in subsection 2.2 in the Supporting Information. Peaks intensity and position are summarized in **Table S2** of the Supporting Information for the N117 Membrane, the ND- Vulcan Nafion electrode and the ND-Vulcan Aquivion electrode while **Figure S3** presents results on the Aquivion ND- Vulcan electrode. Results are in close agreement with literature on bulk ionomer structure. At a given relative humidity condition, extracted peaks positions shift to higher q when decreasing the equivalent weight from N117 membrane, 0.17 $Å^{-1}$ (1100 EW), to Nafion ND- Vulcan electrode, 0.20 $Å^{-1}$ (1000 EW) until Aquivion ND- Vulcan electrode, 0.21 $Å^{-1}$ (835 EW). From ionomers swelling laws, the estimated lamellae thickness decreases with ionomer equivalent weight from 32 Å for N115 (1100 EW), to 26 Å for Nafion (1000 EW) in electrode, down to 22 Å for Aquivion (835 EW) in electrode. Thus, at 94% relative humidity, the hydrophilic domains inside Nafion and Aquivion ionomers are respectively 6.3 and 7.8 Å thick in average.

$$\%wt = \frac{th_{water}}{th_{water} + \frac{\rho_{ionomer}}{\rho_{water}} . th_{ionomer}} \quad (7)$$

Following the Equation 7, we retrieved an ionomer weight water uptake of 20% and 26%, respectively, which are close from the water sorption measurement performed on Nafion coating (1000 EW). Indeed, isotherm sorption curve presented on **Figure S4** shows a weight water uptake of 25% for Nafion (1000 EW) at 95% relative humidity.

Based on ionomer peak evolution with hydration and sorption measurements, results showed that ionomer contained in ND- Vulcan electrode and bulk ionomer are similar: they have a close nanostructure and swelling law. It was said in the introduction that ionomer inside the catalyst layer disperses as thin film or as aggregates. Results on ND- Vulcan electrode suggest that ionomer peak results from diffraction inside aggregates, which are bulk like material with numerous ordered nanophase separation. On the other hand, looking at scattering profiles of D- Vulcan electrode on **Figure 2-a**, one can see that peaks positions and shapes are dramatically different. Both electrodes were made with the exact same composition but with a different manufacturing process. There is no doubt that peaks on the profiles of D- Vulcan electrode result from ionomer but it is not an ionomer peak resulting from diffraction of ionomer bundles. Indeed, assuming that the peak observed on D- Vulcan electrode results from diffraction and

considering 26 Å thick lamellae, we estimate that ionomer should have 62% weight water uptake at 94 % relative humidity. Such an excessive water uptake has never been observed on bulk Nafion in this range of temperature and humidity conditions. This is an evidence showing that the peak related to the ionomer structure from D- Vulcan electrode does not result from bulk ionomer aggregates but from another ionomer structure, which is probably an ionomer thin film spread around the catalyst. This assumption has been checked by Transmission Electronic Microscopy. Elemental Fluorine EDS mapping presented in section 5 of the Supporting Information confirms that ionomer forms large aggregates of several hundreds of nanometers inside the D- HSA electrode. At the opposite, fluorine mapping on a well-dispersed electrode shows a homogeneous ionomer distribution at the carbon surface.

3.2. Ionomer thin film structure and water distribution inside the electrode

We will simulate 1D SANS profiles of ideal structures in order to study the ionomer structure and its distribution inside D- Vulcan and D- HSA electrodes. In the literature, microscopy studies[1,46] show that despite its relative high roughness, carbon primary particles can be considered as sphere-like structures covered by an ionomer layer with a dry polymer film thickness of 2 to 3 nm thick according to Park *et al.*[46] Koizumi *et al.*[47] have used a simple core shell model in order to analyze their SANS profiles on the q range that probes carbon primary particles. Their electrode was hydrated with a solvent having the same SLD as the ionomer in order to merge the ionomer and the water scattering contributions. Thus, they could not resolve the water location. However, several works on ionomer thin film[2,24] showed that condensed water appears at the Pt/ionomer interface. Ueda *et al.*[2] shown the presence of a 3 Å thick water film between a reconstructed Nafion thin film (400 Å thick) over a flat platinum surface using Grazing Incident Small Angle Neutron Scattering (GISANS). Besides, sorption isotherms measurements performed on carbons (HSA and Vulcan) showed that water uptake by carbon increases with relative humidity (Sorption isotherm of **Figure S5**). Those results shows that carbon rough surface must adsorb water even without ionomer. In addition, sorption isotherms of catalyst made with the same carbons support revealed that catalyst uptake even more water (Sorption isotherm of **Figure S6**). This behavior is probably due to the hydrophilic nature of platinum.

Taking into account the results previously published, our scattering profiles were then fitted with different models of core shell structures presented in **Figure 3-a**. In the first one, named "hydrated ionomer model", the spheres of carbon are covered with a hydrated ionomer film with variable thickness and SLD, depending on its hydration. Indeed, SLD of the hydrated

ionomer is supposed to decrease with water uptake, considering their respective SLD $4.2.10^{-6}$ $Å^{-2}$ and $-0.56.10^{-6}$ $Å^{-2}$. In the second model, named "inner water layer model", the carbon spheres are covered by a first layer of pure water surrounding by a second layer of dry ionomer, that do not uptake water. The last one, named "porous carbon surface" considers that water may fill carbon surface pores creating an outer carbon layer of variable thickness and SLD, this particle is then covered by a pure water layer and a dry ionomer shell. Nevertheless, our models are supposed to depict the organisation of the Pt/C and ionomer interface, even if we consider only a single type of interface because of the small contribution of Platinum to scattering profiles. At the q range were correlation appears, SANS intensity probes the electrode structure at the scale of few nanometers. Models are then used to fit correlation peak and to study the water and ionomer shells at the catalyst surface. Since, at this q range, scattering intensity results from neutrons interferences on few nanometres, apparition of the correlation peak does not require primary carbon particles to be fully covered by water and ionomer. Indeed, carbon particles sizes are much larger, around 20 to 50 nm of diameter, than the structure scale probed at this q range. Correlation peaks result from shells structures present locally at the carbon surface but which is not necessary homogeneously dispersed.

At the q range where correlation peak appears, shape and size of carbon particle does not affect strongly the position of the correlation peak since profiles intensity probes shells organization and sizes at the carbon surface, which are very small compared to carbon particles diamater. However, models require a carbon particles average size that is known from literature. Padgett *et al.*[48] studied Vulcan carbon and showed that, in average, primary particles radius are around 135 Å. In fact, Vulcan particles split in two populations with different diameter 10-20 nm and 25-40 nm. HSA carbon presents also distinct primary particles types, one with 15-35 nm diameters and a larger one with 20-40 nm that appears partially hollowed. We include in our model some polydispersity in the size of the carbon nanoparticles and in the thicknesses of the ionomer and water shells. Details on models parameters are presented in the subsection 4 of the Supporting Information.

Before fitting the correlation peak, incoherent scattering intensity was measured at 0,4 $Å^{-1}$ and subtracted to SANS profiles intensity. As shown by Equation 3 and 4, the form factor P(q) of ideal smooth core shells structures decreases as a q^{-4} function. Hence, correlation peaks observed due to constructive interferences of shells scattering contributions will be amplified by plotting $I(q).q^4$ versus q for ideal smooth core-shell structures. On experimental profiles, slopes observed between 8.10^{-3} and 5.10^{-2} $Å^{-2}$ decreases as a q^{-n} function with a n comprise

between 3 and 4. Experimental profiles were then plotted as $I(q).q^n$ versus q to reveal correlation peaks. Resulting profiles were then fitted on the q range corresponding to the correlation peak (0.07-0.5 $Å^{-1}$) with the core shells form factors of ideal smooth core shells structure multiplied by q^4. Profiles from D- Vulcan and D- HSA and their fits are presented on **Figure 3-a** and **Figure 3-b** respectively. The "hydrated ionomer model" does not fit with experimental data for D- Vulcan and D- HSA electrode. It does not reproduce the experimental correlation peak as shown by the dash grey line plot that is the best fit obtained. Experimental peaks on profiles of D- Vulcan and D- HSA electrodes can only be reproduced with core multishell models considering a condensed water layer between the Pt/C catalyst and the ionomer. Then, extracted water and ionomer shells thicknesses using the "inner water layer model" are shown on **Figure 3-d** as a function of relative humidity for D- Vulcan. Parameters extracted from fitting process are presented in **Table S3** of the Supporting Information. The thickness of the condensed water increases with relative humidity. The ionomer film thickness is estimated to be around 21 Å and it does not seem to absorb water since its SLD does not decrease below 4.2 10^{-6} $Å^{-2}$, which is the dry ionomer SLD. Indeed, with water uptake, the hydrated ionomer SLD would decrease toward -0.56 10^{-6} $Å^{-2}$ (H_2O SLD) depending on the volume of water uptake. It is important to understand that those results do not suggest that ionomer covers the whole carbon support surface. Indeed, at the q range of the correlation peak, neutrons scattering probes scales sizes of few nanometers and not the whole carbon particles. Thus, each fraction of carbon surface covered by water and ionomer would contribute to the correlation peak even if the carbon particle is not fully covered by water and ionomer. Core-shells models fitting shows then the average structure of water and ionomer layers over the volume sample.

The same analysis with the "inner water layer model" was performed on D- HSA electrode and fitting of experimental curves are presented on **Figure S8** of the Supporting Information while **Table S4** summarizes fitted parameters. Using this "inner water layer model", the water film thickness estimated around 5 Å for D- HSA electrode was much lower than for D- Vulcan electrode. Now, we know from water sorption measurements, presented in **Figure S7** of the Supporting Information, that D- HSA electrode water uptake is more important than D- Vulcan. The literature shows that High Specific Area (HSA) carbon support has a large amount of meso pores, which constitutes more than 50% of its specific surface area[49]. This pores can be filled by water because of capillary condensation that explains the larger water uptake of HSA carbon compared to Vulcan carbon as shown by Pt/C catalysts isotherms presented in **Figure S6** of the Supporting Information. Therefore, the "inner water layer" model does not depict properly the

D- HSA electrode because it does not take into account surface meso porosity and strongly underestimates the water content.

Then, we have to consider that water filling those pores changes the SLD over a certain thickness of the outermost carbon layer. In order to fit properly the data one have to use the "porous carbon surface" model. Fitting profiles of D- HSA electrode gives the parameters values presented on **Figure 3-e**, which are summarized in **Table S5** of the Supporting Information. Ionomer film thickness seems to increase with hydration from 16 to 24 Å while it remains apparently dry (SLD = 4.2 10^{-6} $Å^{-2}$). This could be explained by the deformation of the ionomer film upon catalyst hydration when pores are progressively filled with water pushing out some of ionomer that cover the porous structure on the surface. The pure water film at the catalyst/ionomer interface is estimated around 8 Å while the depth of meso pores filled with water is about 32 Å with an SLD of 3.7 10^{-6} $Å^{-2}$ at 95% relative humidity. Hence, if surface meso porosity is fully filled with H_2O at 95% relative humidity, then pores represent 42% in volume of the carbon outmost layer. Thanks to these results, we can compute the volume of water contained at the carbon particles surface. Then considering the volume of carbon particles and the volume of the several layers, we may retrieve the overall water volume fraction(V_{water}/V_{total}), which is 17% and 23% for D- Vulcan and D- HSA electrodes, respectively. Water sorption isotherms give a water volume content of 12% and 25% for D- Vulcan and D- HSA electrodes. Sorption and SANS measurement are close for D- Vulcan and D- HSA electrode, thus the full amount of water seems to be located at the Pt/C catalyst surface.

In addition, it is interesting to notice that the thickness of the ionomer shell spread over is very close for Vulcan and HSA carbon supports, respectively 21 and 24 Å at 95% RH, and is smaller than the average thickness of 27 Å for hydrophobic lamellae in Nafion 1100 EW membrane. However, Loppinet *et* Gebel[50,51] studied ionomer dispersion in different media by SAXS, considering hydrophobic domains were rodlikes structures (instead of lamellae). They estimate that in average, hydrophobic domains radius were between 17 to 25 Å, which corresponds to the dry ionomer shell thicknesses measured in this study. Therefore, this explains the fact that water is not located inside the ionomer but at the interface between Pt/C catalyst and ionomer. The 34 Å of the total ionomer and water shell thickness retrieved on D- HSA electrode at 95% relative humidity is thinner than the 50 Å found by Koizumi *et al.*[26] by SANS because they did not take into account the scattering contribution of the porous carbon surface. In addition, water film thickness retrieved at the Pt/C catalyst is thicker than estimated by Ueda *et al.*[2] on

a reconstructed Nafion thin film (400 Å thick) over platinum. However, thin film study on smooth substrate may not reproduce what appends in electrode, since the water uptake at the substrate/ionomer interface is an interplay between, material hydrophilicity and substrate/ionomer interaction. Therefore, SANS characterisation afford new additional information on the water and ionomer distribution in catalyst layer and revealed that ionomer thin film and bulk ionomer structures are drastically different. Indeed, in the electrode, ionomer film thickness is in the order of bundle aggregates thicknesses and a water layer appears at the Pt/C catalyst and ionomer interface.

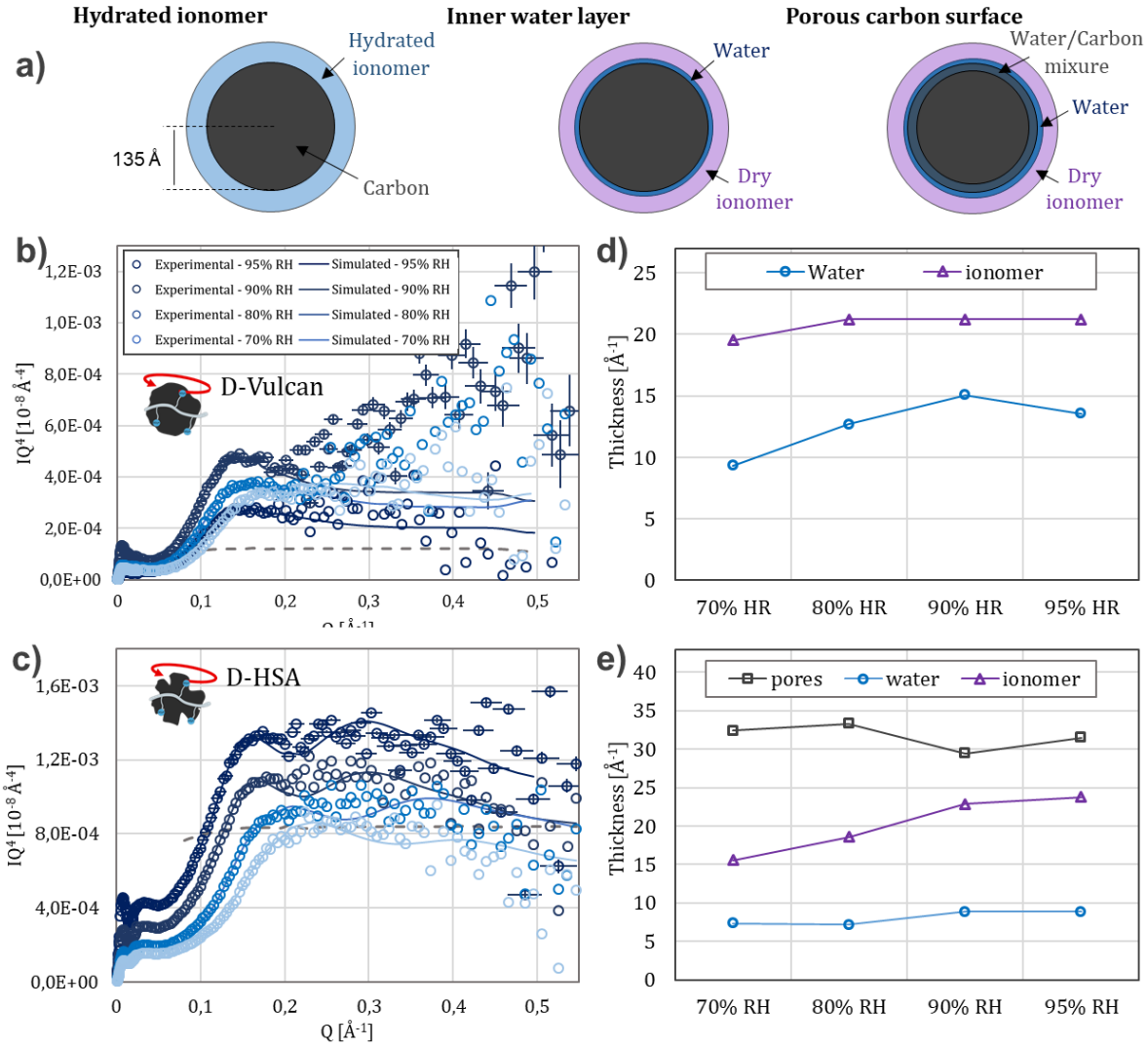

Figure 3. a) Schemes of three models used to reproduce the local structure of the electrodes and more precisely the catalyst, water and ionomer organisation at the nanometer scale. b) Experimental profiles from D- Vulcan and their fitted curves resulting from "inner water layer" model. Dash grey line is the best-fitted curve obtain with "hydrated ionomer" model. Error bar are only reproduced on one scattering profile for clarity. c) Experimental profiles from

D- HSA and their fitted curves resulting from “porous carbon layer” model. Dash grey line is the best-fitted curve obtain with “hydrated ionomer” model. d) Evolution of water and ionomer shells thicknesses with relative humidity. Parameters obtained from “inner water layer” model fitting. Error bars attributed to covariance of fitted parameters are within markers thicknesses e) Estimation of carbon meso pores depth and evolution of ionomer and water shells thicknesses with hydration. Parameters obtained from “porous carbon surface” model fitting. Error bars attributed to covariance of fitted parameters are within markers thicknesses.

To summarize, from the actual knowledge of carbon and electrode structures, we analysed 1D SANS profiles with two different core-shells form factor models to depict the catalyst, water and ionomer organization at the nanometer scale with two different types of carbon, either Vulcan or HSA in the electrode. We highlight that a thin ionomer film of about 20 Å in thickness cover the catalyst and does not seem to swell significantly increasing the relative humidity. This means that, for well dispersed electrodes and for the probed ionomer over carbon weight ratio (I/C) that ranges between 0.67 and 0.8, the ionomer is nearly totally in the form of a thin film coating at least partially the surface of the Carbon particles. There is no significant contribution of scattering due to ionomer aggregates on the SANS profiles. This does not imply necessarily that the whole carbon surface is covered homogeneously and totally by the ionomer. We gave an averaged value for the ionomer film thickness, but there is a polydispersity in thickness of the film, as mentioned above. On the SANS profiles, the intensity of the peak due to the film covering the carbon increases with the ionomer coverage. In addition, there is a thin water film between the Pt/C catalyst and the ionomer even below 100%RH. Its thickness is about 10 Å and is larger than what has been reported at the interface between Pt and ionomer on flat model substrates. It implies that there is also water at the carbon/ionomer interface. In addition, our results strongly suggest the presence of water inside the HSA carbon surface porosity. Further analysis of SANS profiles in the lower q range will confirm those results.

3.4. Validating core shell models with contrast variation

In this section will use the unique advantage of neutrons to perform contrast variation in order to study the organization of water and ionomer at the nanometer scale of the catalyst . Neutrons interaction with light or heavy water is dramatically different and thus, Scattering Lengths Densities (SLD) of water H_2O ($-0.56\ 10^{-6}$ Å^{-2}) and heavy water D_2O ($6.34\ 10^{-6}$ Å^{-2}) are significantly different. In addition, the SLD of H_2O and D_2O are close to air (0 Å^{-2}) and carbon ($6.7\ 10^{-6}$ Å^{-2}) respectively allowing to mask a material contribution to the overall profile.

Hence, with H_2O hydration, air and water contribution are merged together while with D_2O hydration, it is the water and the carbon contribution that are merged together in the resulting SANS scattering profile. We therefore perform scattering experiments on the same samples but having the surrounding media (air) saturated by H_2O and D_2O. Doing so, only the scattering length density of the solvent varies while the catalyst particles are not affected. Obtaining a second contrast within the same state of dispersion and structure will give further confidence on the fine details. **Figure 4 -a** presents experimental profiles obtained from D- Vulcan and D- HSA electrodes. Electrodes hydrated with H_2O have a larger incoherent than those with D_2O. Both profiles exhibit same evolutions with contrast variation. Two main features are observed with D_2O hydration, the correlation peak disappearance, and the decrease of the intensity slope between 0.02 $Å^{-1}$ and 0.06 $Å^{-1}$. The variation of the intensity observed at the lowest q values between H_2O and D_2O profiles highlights this slope evolution. Core shell models used in subsection 3.2 should be able to reproduce profiles evolutions induced by contrast variation. Therefore, we have plotted the ratio of experimental profiles under H_2O and D_2O hydration at 95% relative humidity. In this way, the structure factor of the carbon contribution is erased and the correlation peak is fully revealed. Curves were then fitted with the ratio of the form factors using “inner water layer” model for D- Vulcan profile and “porous carbon surface” model for D- HSA. Again, experimental profiles cannot be reproduced by the model when considering that the ionomer film is hydrated (dash grey line). However, there are well fitted by their respective models and give results in close agreement with those obtain in subsection 3.2. At 95% relative humidity, the estimation of the ionomer shell thickness is 25.3 Å (±0.177 Å) on D- Vulcan and 19.3 Å (±0.306 Å) on D- HSA while meso porosity are estimated at 29.9 Å (±1.68 Å) than previously. Full details are given in subsection 4.3 in the Supporting Information while **Table S6** and **Table S7** present fitted parameters from D- Vulcan and D- HSA electrodes. Finally, results from this contrast variation analysis strengthen our previous conclusion on the structure of carbon primary particles inside both catalysts layers.

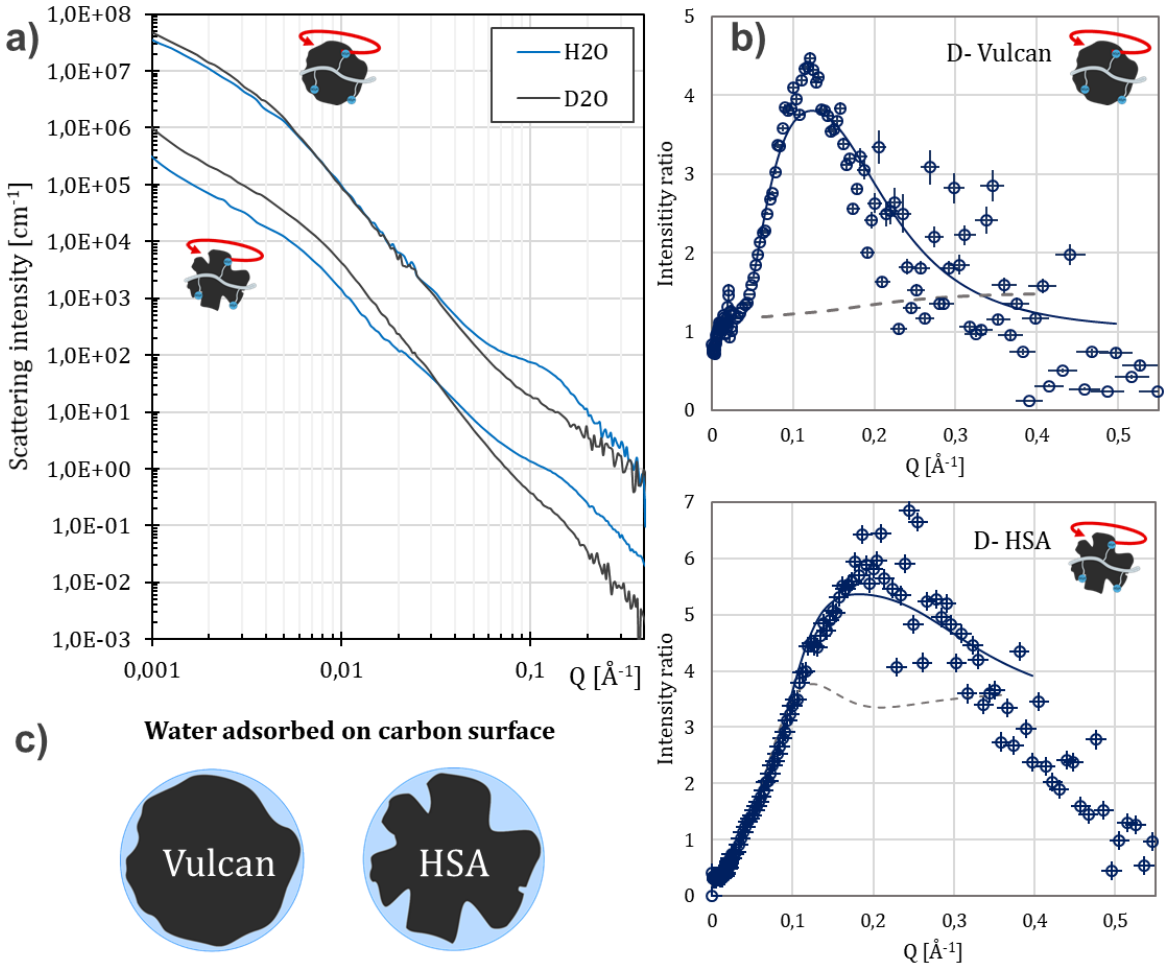

Figure 4. a) 1D SANS profiles evolution with contrast variation of D- Vulcan and D- HSA electrodes. Electrodes hydrated with H_2O and D_2O at 95% RH. H_2O profiles intensities are subtracted from incoherent scattering. b) Ratio of H_2O profile over D_2O profile highlights the correlation peak for D- Vulcan and D- HSA. Experimental ratio fitted with ratio of core shells models using the "inner water layer" model for D- Vulcan and the "porous carbon layer" model for D- HSA. Dash grey lines are the best fit obtained considering a shell made from hydrated ionomer instead of water and ionomer layers. c) Schemes of adsorbed water at the surface of Vulcan and HSA carbon supports with water filling HSA carbon meso porosity.

3.5 Using contrast variation to reveal the carbon support structure

On **Figure 4-a**, important differences are observed from one electrode to another pointing out the structure evolutions induced by the carbon supports used; either Vulcan or High Surface Area (HSA) carbon supports. Then, contrast variation is used to reveal structural differences between the two electrodes. Since SLDs of air and H_2O are very close, these carbon particles

will scatter neutrons similarly when dispersed in water or in air. Therefore, once hydrated with H_2O, 1D SANS profiles probe specifically the carbon particles. According to Porod law[52], the slope observed with H_2O profiles between 0.02 $Å^{-1}$ and 0.06 $Å^{-1}$ characterizes the carbon surface roughness. Ideal smooth spheres would present a slope decreasing as a q^{-4} function while smaller power values between 3 and 4 characterize rougher surfaces. Profiles intensity from D- Vulcan electrode decreases as a $q^{-3.9}$ function while it does as a $q^{-3.1}$ for D- HSA electrode. This is in accordance with the higher roughness of HSA carbon compared to Vulcan. Then, replacing H_2O with D_2O increases the water SLD close to the carbon SLD value ($6.34.10^{-6}$ $Å^{-2}$ for D_2O against $6.5.10^{-6}$ $Å^{-2}$ for carbon). Thus, carbon and D_2O, having similar SLDs, would scatter as the same material. Looking at D- Vulcan electrode profiles on the **Figure 4-b**, using D_2O for sample hydration instead of H_2O has little effect on the slope which means that adsorbed water at the carbon surface does not change its apparent roughness. However, the D- HSA electrode profile slope increases from $q^{-3.1}$ with H_2O hydration to $q^{-3.9}$ with D_2O as if the surface of carbon becomes smoother due to the presence of D_2O. This can be ascribed to the incorporation of water inside the surface meso pores of the carbon as represented on **Figure 4- c**. Profiles recorded from catalyst alone, 50% weight Pt over HSA carbon, are presented on **Figure S9-a** of the Supporting Information. They showed the same increase of slopes with D_2O hydration suggesting that carbon surface meso pores are filled with D_2O even without ionomer. Those results confirm the presence of meso pores at the HSA carbon support surface, which are filled by water through capillary condensation and are responsible for the high water uptake of D- HSA electrode. Our study shows that a water thin film appears between the Pt/C catalyst and the ionomer film. SANS profiles were also recorded on a sample made only with HSA carbon and ionomer (without platinum), which are presented on **Figure S9-b** of the Supplement Information. SANS profile of the sample hydrated at 95%RH shows a correlation peak around 0.12 $Å^{-1}$. Therefore, even if there is no platinum, ionomer disperses as a thin film at the carbon surface and a water layer appears again between ionomer and carbon. All those results shows that ionomer disperses at the Pt/C catalyst surface and that a water layer appears both at the carbon/ionomer and platinum/ionomer interfaces.

Slopes inflexions at lower q values, around 0.005 $Å^{-1}$ give information on carbon network structure. Below the inflexion location, scattered intensity characterizes the primary particles while above it characterizes the catalyst layer aggregates. On **Figure 4-a**, inflexion appears at higher q values for the D- Vulcan catalyst layer (4.10^{-3} $Å^{-1}$) than for D- HSA (6.10^{-3} Å). The upturn position is related to the volume average of particles characteristic sizes over the entire

electrode volume illuminated by the beam. Therefore, carbon particles mean diameter appears 20% larger for Vulcan carbon. In addition, below 4.10^{-3} $Å^{-1}$, differences in experimental profiles slopes witness that the structure of catalyst layer aggregates are radically different from one electrode to another.

4. Conclusion

In this paper, we propose a detailed method to characterize the structure of the catalyst layer in a large range of length scales from nm to hundreds of nm through an analysis method of 1D Small Angle Neutron (SANS) profiles with contrast variation. Catalyst layers differing in composition, either in types of ionomer or carbon support, but also in fabrication process. It shows how powerful the SANS is to get information on the structure of the catalyst layer. This is the only method that could offer such quantitative and detailed information on water distribution and ionomer structure.

The analysis of the 1D SANS profiles in a wide q range with contrast variation reveals the presence of ionomer as aggregates or as thin film coating the Pt/C catalyst depending on the manufacturing process. When stacked in the pores of the catalyst layer, the size of the ionomers aggregates appears to be larger than 50 nm up to several hundreds of nanometers. Their structure and swelling behavior are very similar to that of the bulk ionomer in the membrane . However, once ionomer disperses as thin film, 1D SANS profiles exhibit a drastically different feature with a correlation peak whose shape and position depend on the relative humidity. All the profiles obtained with the different catalyst layer compositions can be fitted with a form factor of a core multi-shell model allowing extracting information on the ionomer thin film thickness and water location and content. To summarize, a 20 to 30 Å thick ionomer shell coats the Pt/C catalyst made from Vulcan or High Surface Area Carbon (HSAC) support. For both catalyst, condensed water appeared at the ionomer/catalyst interface, even under 100% relative humidity. However, there are differences between smooth spherical particles from Vulcan and the rough and porous spherical particles from HAS carbon. In the case of HSA carbon support, the volume of condensed water at the carbon/ionomer interface is larger than for Vulcan carbon support because water fills the HSA carbon meso pores due to capillary condensation.

SANS method paves the way toward a more refined understanding of the structure/properties relationship of the electrode. It shows how the structure of the carbon support of the Pt/C

catalyst influences the ionomer and the water dispersions, and it can explain why the HSAC offers better performance. Indeed, these conclusions drawn from ex-situ measurements can most probably be extrapolated to what happens during PEMFC operation with water being primarily located in the pores of the carbon and at the Pt/C catalyst/ionomer interface before filling larger pores.

Furthermore, the same SANS profile analysis can be applied to various catalyst layers used in fuel cells or electrolysers (PEME, AEMFC, AEME, DMFC…) that used nanoscale structured electrodes Thus, this works provide to the scientific community original tool and crucial information to understand the fuel cell operation that are not accessible through other methods than SANS.

Supporting Information

Details on the manufacturing process and composition of the electrodes, details on the SANS models, analyses and results of the models, water vapor sorption isotherms, STEM imaging of the ionomer in the electrodes.

Corresponding author

Arnaud MORIN, CEA - Liten
arnaud.morin@cea.fr

Author Contribution

The manuscript was written through contributions of all authors. All authors have given approval to the final version of the manuscript.

Acknowledgements

This work has partially received funding from the Fuel Cells and Hydrogen 2 Joint Undertaking under grant agreement No. 875025 (FURTHER-FC project). This Joint Undertaking receives support from theEuropean Union's Horizon 2020 Research and Innovation programme, Hydrogen Europe and Hydrogen Europe Research[31]. We especially thank Toyota Motor Europe for manufacturing and providing MEA.
Authors thanks the Institut Laue Langevin (ILL), Grenoble and the D22 beam line for they contribution to this study[32,33].
This work benefited from the use of the SasView application, originally developed under NSF award DMR-0520547. SasView contains code developed with funding from the European

Union's Horizon 2020 research and innovation programme under the SINE2020 project, grant agreement No 654000.

References

1. Guetaz, L., Lopez-Haro, M., Escribano, S., Morin, A., Gebel, G., Cullen, D.A., More, K.L., et Borup, R.L. (2015) Catalyst-Layer Ionomer Imaging of Fuel Cells. *ECS Trans.*, **69** (17), 455.
2. Ueda, S., Koizumi, S., Ohira, A., Kuroda, S., et Frielinghaus, H. (2018) Grazing-incident neutron scattering to access catalyst for polymer electrolyte fuel cell. *Physica B: Condensed Matter*, **551**, 309-314.
3. Morawietz, T., Handl, M., Oldani, C., Friedrich, K.A., et Hiesgen, R. (2018) Influence of Water and Temperature on Ionomer in Catalytic Layers and Membranes of Fuel Cells and Electrolyzers Evaluated by AFM. *Fuel Cells*, **18** (3), 239-250.
4. Gebel, G. (2000) Structural evolution of water swollen perfluorosulfonated ionomers from dry membrane to solution. *Polymer*, **41** (15), 5829-5838.
5. Salari, S., Stumper, J., et Bahrami, M. (2018) Direct measurement and modeling relative gas diffusivity of PEMFC catalyst layers: The effect of ionomer to carbon ratio, operating temperature, porosity, and pore size distribution. *International Journal of Hydrogen Energy*, **43** (34), 16704-16718.
6. Salari, S., Tam, M., McCague, C., Stumper, J., et Bahrami, M. (2020) The ex-situ and in-situ gas diffusivities of polymer electrolyte membrane fuel cell catalyst layer and contribution of primary pores, secondary pores, ionomer and water to the total oxygen diffusion resistance. *Journal of Power Sources*, **449**, 227479.
7. Yarlagadda, V., Carpenter, M.K., Moylan, T.E., Kukreja, R.S., Koestner, R., Gu, W., Thompson, L., et Kongkanand, A. (2018) Boosting Fuel Cell Performance with Accessible Carbon Mesopores. *ACS Energy Lett.*, **3** (3), 618-621.
8. Kongkanand, A., et Mathias, M.F. (2016) The Priority and Challenge of High-Power Performance of Low-Platinum Proton-Exchange Membrane Fuel Cells. *J. Phys. Chem. Lett.*, **7** (7), 1127-1137.
9. Karan, K. (2019) Interesting Facets of Surface, Interfacial, and Bulk Characteristics of Perfluorinated Ionomer Films. *Langmuir*, **35** (42), 13489-13520.
10. Nonoyama, N., Okazaki, S., Weber, A.Z., Ikogi, Y., et Yoshida, T. (2011) Analysis of Oxygen-Transport Diffusion Resistance in Proton-Exchange-Membrane Fuel Cells. *J. Electrochem. Soc.*, **158** (4), B416.
11. Heinzmann, M., Weber, A., et Ivers-Tiffée, E. (2019) Impedance modelling of porous electrode structures in polymer electrolyte membrane fuel cells. *Journal of Power Sources*, **444**, 227279.
12. Neyerlin, K.C., Gu, W., Jorne, J., Clark, A., et Gasteiger, H.A. (2007) Cathode Catalyst Utilization for the ORR in a PEMFC: Analytical Model and Experimental Validation. *J. Electrochem. Soc.*, **154** (2), B279.
13. Young, A.P., Stumper, J., et Gyenge, E. (2009) Characterizing the Structural Degradation in a PEMFC Cathode Catalyst Layer: Carbon Corrosion. *J. Electrochem. Soc.*, **156** (8), B913-B922.
14. Kreuer, K.D., Schuster, M., Obliers, B., Diat, O., Traub, U., Fuchs, A., Klock, U., Paddison, S.J., et Maier, J. (2008) Short-side-chain proton conducting perfluorosulfonic acid ionomers: Why they perform better in PEM fuel cells. *Journal of Power Sources*, **178** (2), 499-509.

15. Kreuer, K.-D., et Portale, G. (2013) A Critical Revision of the Nano-Morphology of Proton Conducting Ionomers and Polyelectrolytes for Fuel Cell Applications. *Advanced Functional Materials*, **23** (43), 5390-5397.
16. Gebel, G., et Lambard, J. (1997) Small-Angle Scattering Study of Water-Swollen Perfluorinated Ionomer Membranes. *Macromolecules*, **30** (25), 7914-7920.
17. Martinez, N., Porcar, L., Escribano, S., Micoud, F., Rosini, S., Tengattini, A., Atkins, D., Gebel, G., Lyonnard, S., et Morin, A. (2019) Combined Operando High Resolution SANS and Neutron Imaging Reveals in-Situ Local Water Distribution in an Operating Fuel Cell. *ACS Appl. Energy Mater.*, **2** (12), 8425-8433.
18. Kusoglu, A., et Weber, A.Z. (2017) New Insights into Perfluorinated Sulfonic-Acid Ionomers. *Chem. Rev.*, **117** (3), 987-1104.
19. Kusoglu, A., Dursch, T.J., et Weber, A.Z. (2016) Nanostructure/Swelling Relationships of Bulk and Thin-Film PFSA Ionomers. *Advanced Functional Materials*, **26** (27), 4961-4975.
20. DeCaluwe, S.C., Baker, A.M., Bhargava, P., Fischer, J.E., et Dura, J.A. (2018) Structure-property relationships at Nafion thin-film interfaces: Thickness effects on hydration and anisotropic ion transport. *Nano Energy*, **46**, 91-100.
21. Uchida, M. (2020) PEFC catalyst layers: Effect of support microstructure on both distributions of Pt and ionomer and cell performance and durability. *Current Opinion in Electrochemistry*, **21**, 209-218.
22. Sharma, R., et Andersen, S.M. (2018) Quantification on Degradation Mechanisms of Polymer Electrolyte Membrane Fuel Cell Catalyst Layers during an Accelerated Stress Test. *ACS Catal.*, **8** (4), 3424-3434.
23. Woo, S., Lee, S., Taning, A.Z., Yang, T.-H., Park, S.-H., et Yim, S.-D. (2020) Current understanding of catalyst/ionomer interfacial structure and phenomena affecting the oxygen reduction reaction in cathode catalyst layers of proton exchange membrane fuel cells. *Current Opinion in Electrochemistry*, S2451910320300636.
24. Wood, D.L., Chlistunoff, J., Majewski, J., et Borup, R.L. (2009) Nafion Structural Phenomena at Platinum and Carbon Interfaces. *J. Am. Chem. Soc.*, **131** (50), 18096-18104.
25. Gilbert, J.A., Kariuki, N.N., Subbaraman, R., Kropf, A.J., Smith, M.C., Holby, E.F., Morgan, D., et Myers, D.J. (2012) In Situ Anomalous Small-Angle X-ray Scattering Studies of Platinum Nanoparticle Fuel Cell Electrocatalyst Degradation. *J. Am. Chem. Soc.*, **134** (36), 14823-14833.
26. Koizumi, S., Ueda, S., Inada, T., Noda, Y., et Robinson, R.A. (2019) Microstructure and water distribution in catalysts for polymer electrolyte fuel cells, elucidated by contrast variation small-angle neutron scattering. *J Appl Crystallogr*, **52** (4), 791-799.
27. Lee, J., Escribano, S., Micoud, F., Gebel, G., Lyonnard, S., Porcar, L., Martinez, N., et Morin, A. (2020) In Situ Measurement of Ionomer Water Content and Liquid Water Saturation in Fuel Cell Catalyst Layers by High-Resolution Small-Angle Neutron Scattering. *ACS Appl. Energy Mater.*, **3**, 8393-8401.
28. Yoshimune, W., et Harada, M. (2019) Effect of Pt Loading on the Adsorption of Perfluoro-sulfonic Acid Ionomer in Catalyst Ink for Polymer Electrolyte Fuel Cells. *Chem. Lett.*, **48** (5), 487-490.
29. Kobayashi, A., Fujii, T., Harada, C., Yasumoto, E., Takeda, K., Kakinuma, K., et Uchida, M. (2021) Effect of Pt and Ionomer Distribution on Polymer Electrolyte Fuel Cell Performance and Durability. *ACS Appl. Energy Mater.*, **4** (3), 2307-2317.
30. Harada, M., Takata, S., Iwase, H., Kajiya, S., Kadoura, H., et Kanaya, T. (2021) Distinguishing Adsorbed and Deposited Ionomers in the Catalyst Layer of Polymer

Electrolyte Fuel Cells Using Contrast-Variation Small-Angle Neutron Scattering. *ACS Omega*, **6** (23), 15257-15263.
31. European Project Further-FC. www.*https://further-fc.eu/*. Accessed the 06/05/2021
32. Morin, A., Chabot, F., Gebel, G., Jacqmin, L., Lyonnard, S., Micoud, F., Porcar, L., Roiron, C., Rosini, S., Toudret, P., Et Vandenberghe, F. (2020) Nanostructure of ionomer in fuel cell electrodes by SANS. [Data Set]. *Institut Laue-Langevin (ILL)*. https://doi.ill.fr/10.5291/ILL-DATA.9-12-595
33. Morin, A., Chabot, F., Escribano, S., Lee, J., Micoud, F., Porcar, L., Et Vandenberghe, F. (2019) Operando fuel cell structural studies. *Institut Laue-Langevin (ILL)*. https://doi.ill.fr/10.5291/ILL-DATA.TEST-2991
34. D22 Beamline. *https://www.ill.eu/users/instruments/instruments-list/d22/description/instrument-layout*. Accessed the 09/05/2021.
35. Grasp - ILL Neutrons for Society. *https://www.ill.eu/users/support-labs-infrastructure/software-scientific-tools/grasp/*. Accessed the 09/05/2021.
36. Hammouda, B. (2016) Probing nanoscale structures - The SANS toolbox. NIST - Center for Neutron Research, Gaithersburg, USA. 717. *https://www.ncnr.nist.gov/staff/hammouda/the_SANS_toolbox.pdf*
37. Balu, R., Choudhury, N.R., Mata, J.P., de Campo, L., Rehm, C., Hill, A.J., et Dutta, N.K. (2019) Evolution of the Interfacial Structure of a Catalyst Ink with the Quality of the Dispersing Solvent: A Contrast Variation Small-Angle and Ultrasmall-Angle Neutron Scattering Investigation. *ACS Appl. Mater. Interfaces*, **11** (10), 9934-9946.
38. Yoshimune, W., et Harada, M. (2019) Effect of Pt Loading on the Adsorption of Perfluoro-sulfonic Acid Ionomer in Catalyst Ink for Polymer Electrolyte Fuel Cells. *Chem. Lett.*, **48** (5), 487-490.
39. SASView Software. *https://www.sasview.org/*. Accessed the 12/05/2021.
40. Guinier, A., et Fournet, G. (1955) Small angle scattering of X-rays. A. Guinier and G. Fournet. *John Wiley and Sons*, 268.
41. Cullen, D.A., Koestner, R., Kukreja, R.S., Liu, Z.Y., Minko, S., Trotsenko, O., Tokarev, A., Guetaz, L., Meyer, H.M., Parish, C.M., et More, K.L. (2014) Imaging and Microanalysis of Thin Ionomer Layers by Scanning Transmission Electron Microscopy. *J. Electrochem. Soc.*, **161** (10), F1111.
42. Rubatat, L., Gebel, G., et Diat, O. (2004) Fibrillar Structure of Nafion: Matching Fourier and Real Space Studies of Corresponding Films and Solutions. *Macromolecules*, **37** (20), 7772-7783.
43. Morin, A., Gebel, G., Porcar, L., Peng, Z., Martinez, N., Guillermo, A., et Lyonnard, S. (2016) Quantitative Multi-Scale Operando Diagnosis of Water Localization inside a Fuel Cell. *J. Electrochem. Soc.*, **164** (2), F9.
44. Ohma, A., Mashio, T., Sato, K., Iden, H., Ono, Y., Sakai, K., Akizuki, K., Takaichi, S., et Shinohara, K. (2011) Analysis of proton exchange membrane fuel cell catalyst layers for reduction of platinum loading at Nissan. *Electrochimica Acta*, **56** (28), 10832-10841.
45. Ryong-Joon Roe (2001) Methods of X-Ray and Neutron Scattering in Polymer Science. *Oxford University Press, New York*.
46. Park, Y.-C., Tokiwa, H., Kakinuma, K., Watanabe, M., et Uchida, M. (2016) Effects of carbon supports on Pt distribution, ionomer coverage and cathode performance for polymer electrolyte fuel cells. *Journal of Power Sources*, **315**, 179-191.
47. Koizumi, S., Ueda, S., Inada, T., Noda, Y., et Robinson, R.A. (2019) Microstructure and water distribution in catalysts for polymer electrolyte fuel cells, elucidated by contrast variation small-angle neutron scattering. *J Appl Cryst*, **52** (4), 791-799.
48. Padgett, E., Andrejevic, N., Liu, Z., Kongkanand, A., Gu, W., Moriyama, K., Jiang, Y., Kumaraguru, S., Moylan, T.E., Kukreja, R., et Muller, D.A. (2018) Editors' Choice—

Connecting Fuel Cell Catalyst Nanostructure and Accessibility Using Quantitative Cryo-STEM Tomography. *J. Electrochem. Soc.*, **165** (3), F173-F180.
49. Soboleva, T., Malek, K., Xie, Z., Navessin, T., et Holdcroft, S. (2011) PEMFC Catalyst Layers: The Role of Micropores and Mesopores on Water Sorption and Fuel Cell Activity. *ACS Appl. Mater. Interfaces*, **3** (6), 1827-1837.
50. Loppinet, B., Gebel, G., et Williams, C.E. (1997) Small-Angle Scattering Study of Perfluorosulfonated Ionomer Solutions. *J. Phys. Chem. B*, **101** (10), 1884-1892.
51. Loppinet, B., et Gebel, G. (1998) Rodlike Colloidal Structure of Short Pendant Chain Perfluorinated Ionomer Solutions. *Langmuir*, **14** (8), 1977-1983.
52. Chiang, W.-S., Chen, J.-H., et Liu, Y. (2019) Investigation of porous materials with large surface heterogeneity using the generalized Porod's scattering law method. *Phys. Rev. E*, **99** (4), 042801.

Detailed catalyst layer structure of Proton Exchange Membrane Fuel Cell from contrast variation small-angle neutron scattering

PEMFC catalyst layer operation is closely related to its nanoscale structure and its water uptake, which were revealed by Small Angle Neutron Scattering (SANS). 1D SANS profiles analysis allowed to probe catalyst layer structure, revealing the ionomer distribution (as aggregates or as thin film), the water uptake and its location. This study revealed that condensed water accumulates at the carbon/ionomer interface or inside porous particles depending on the type of carbon support used.

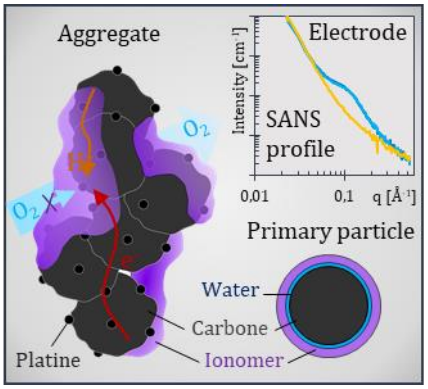

Figure. Complex heterogeneous structure of catalyst layer probed by SANS. Scheme of the critical role of the ionomer distribution on catalyst layer operation at the aggregates scale. 1D SANS profile from electrode and the associated scheme of the primary particle structure revealed by profiles analysis.